PHYSICAL REVIEW A **82**, 061602(R) (2010)

Precisely mapping the magnetic field gradient in vacuum with an atom interferometer

Min-Kang Zhou, Zhong-Kun Hu,* Xiao-Chun Duan, Bu-Liang Sun, Jin-Bo Zhao, and Jun Luo
School of Physics, Huazhong University of Science and Technology, Wuhan 430074, People's Republic of China
(Received 2 August 2010; published 10 December 2010)

The magnetic field gradient has been measured with an atom interferometer using the magnetic sublevels of ^{87}Rb atoms. The Doppler-insensitive measurement effectively eliminates the contribution from gravity and background vibration noise, and the differential measurement also can reject some systematic errors. A resolution of 300 pT/mm has been demonstrated with a 90-s integration time and a spatial resolution of 1.4 mm. The gradiometer was then used to measure the magnetic field gradient in an ultrahigh-vacuum environment. The technique will also be very useful to subtract the systematic error arising from the magnetic field inhomogeneity in precision atom-interferometry experiments, such as gravity measurement.

DOI: 10.1103/PhysRevA.82.061602 PACS number(s): 37.25.+k, 07.55.Ge

Magnetic gradiometers with high sensitivity and spatial resolution have been widely applied in earth's magnetic field mapping, detection of natural resources [1–3], biomagnetism [4], and fundamental physical experiments [5]. The superconducting quantum interference device (SQUID) gradiometer comprising two SQUID magnetometers with a baseline of 4 cm reached an ultrahigh sensitivity of 60 fT/(m $\mathrm{Hz}^{1/2}$) at a frequency of 0.3 Hz [3]. Atomic magnetometers based on nonlinear magneto-optical rotation or the coherent population trapping method have been realized by several groups [6,7]. Gradiometers with atomic magnetometers are also demonstrated at baselines of 25 [8] and 15 mm [9].

In recent years, atom interferometers have proven to be increasingly valuable sensors for the precision measurement of gravitational acceleration and rotation [10,11], the gravitational constant G [12,13], the scalar Aharonov-Bohm effect [14], the fine structure constant [15], and the gravitational red shift [16]. The atom's acceleration due to the interaction between atom and magnetic field was proposed to be measured based on the atom-interferometry technique suggested by F. A. Narducci *et al.* [17,18]. However, it is difficult to distinguish the magnetic effect from gravity and the seismic vibration background in principle. The magnetic-field-sensitive Raman transition (RT) method with π pulse was used to directly measure the magnetic field in an atom interferometer for determining the systematic effect due to the magnetic field inhomogeneity [19].

In this paper, an atom interferometer constructed in a Doppler-insensitive but magnetic-field-sensitive configuration is described to measure the magnetic field gradient directly. The magnetic gradient experienced by the atoms in their trajectories are then encoded in the atom interferometer's phase. As will be shown, contribution to the phase of the gravity and seismic vibration can be neglected in the present work with the copropagating Raman beams, and the differential interferometry signals of each magnetic sublevel are used to extract the magnetic gradient signal and suppress some systematic errors.

The principle of Raman pulse atom interferometry has been described by several groups for gravity measurements and other inertial sensors [20,21]. However, the magnetic-field-insensitive states with magnetic quantum number $m_F = 0$ were chosen to avoid the first-order Zeeman effect in those measurements. For measuring the magnetic field gradient, we choose the nonzero magnetic quantum number atom interferometer to measure the phase due to the magnetic field inhomogeneity. Considering the $D2$ line of ^{87}Rb atom as shown in Fig. 1(a), we choose the ground hyperfine states $|F = 1, m_F = 1\rangle$ and $|F = 2, m_F = 1\rangle$ and excited states $|5\,^2P_{3/2}\rangle$ as a three-level Λ system. The interstate transition is realized by coupling with the phase-locked Raman lasers. For a large detuning Δ from the excited states, the three-level atom can be treated as a two-level atom, and the laser field may be considered to have an effective wave vector $\vec{k}_{\mathrm{eff}} = \vec{k}_1 - \vec{k}_2$. The atoms are coherently driven between the ground hyperfine states by a two-photon Raman transition to form a Rabi oscillation. The tools for manipulating the wave packets in the atom interferometer are $\pi/2$ Raman pulse as a 50:50 beam splitter and π pulse as a reflector. We consider a free-falling atom with initial state $|F = 1, m_F = 1\rangle$ as shown in Fig. 1(b). First, a $\pi/2$ pulse with duration τ is applied to the atoms, and the atoms are driven to the superposition state of $|F = 1, m_F = 1\rangle$ and $|F = 2, m_F = 1\rangle$ with 50% probability for each state. Second, after T time free evolution, the atom's hyperfine states are inversed via exposure to a π pulse with duration 2τ. Finally, another $\pi/2$ pulse is used to recombine the wave packets for observing the interference signal. The probability of an atom in state $|F = 2, m_F = 1\rangle$ after the sequence of $\pi/2 - \pi - \pi/2$ Raman pulses is $P = (1 - \cos\phi)/2$, where the interference phase ϕ for a free-falling atom is $\phi = \phi_L + \phi_g + \phi_B + \phi_o$, where ϕ_L is the Raman-laser-induced phase, ϕ_g is the local gravity acceleration g-induced phase, ϕ_B is the magnetic-field-induced phase, and ϕ_o is the other-physical-effects-induced phase.

For the configuration of an atom interferometer shown in Fig. 1(b), and in the case of the copropagating Raman beams (Doppler-insensitive case), the magnetic-field-induced phase is

$$\phi_B = \frac{\mu_B}{\hbar}(g_{F'} m_F - g_F m_F)\left[\int_0^T B(t)\,dt - \int_T^{2T} B(t)\,dt\right], \tag{1}$$

where μ_B is the Bohr magneton, $g_F(g_{F'})$ are the g factors for ^{87}Rb ground state $|F = 1, m_F = 1\rangle$ ($|F = 2, m_F = 1\rangle$), and

*zkhu@mail.hust.edu.cn

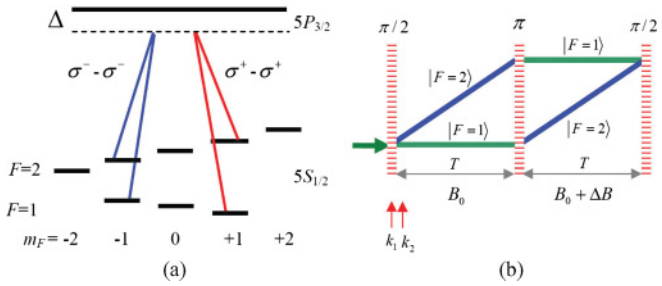

FIG. 1. (Color online) (a) ^{87}Rb magnetic sublevels and Raman beam configuration; (b) interferometry sequence $\pi/2 - T - \pi - T - \pi/2$ and the magnetic field experienced by the atoms.

$\frac{\mu_B}{\hbar} g_{F'} m_F = -\frac{\mu_B}{\hbar} g_F m_F = 0.70$ MHz/G [22], which is denoted as β in the following text. Considering that the variation of the magnetic field is linear in a small atom's free-falling region, the phase due to the magnetic field can be written as $\phi_B = 2\beta\Delta BT$. It means that the atom interferometer can be used to measure the magnetic field gradient. For a typical value of $\Delta B = 200\ \mu G$ and $T = 1$ ms, ϕ_B is estimated to be 1.7 rad, while the gravity-induced phase $\phi_g = (k_1 - k_2)gT^2$ is only at the 10^{-3} rad level, so this atom interferometer is relatively insensitive to gravity and background vibration noise and sensitive to the magnetic field gradient. However, it is not easy to extract ϕ_B from the interferometer total phase ϕ, which is a sum of ϕ_L,ϕ_B, and ϕ_o. Fortunately, for an atom interferometer of $m_F = -1$ atoms interacting with $\sigma^- - \sigma^-$ polarization Raman beams as shown in Fig. 1(a), the phase due to magnetic field is $-\phi_B$, while ϕ_L and ϕ_o are almost the same as those of the $m_F = 1$ state with $\sigma^+ - \sigma^+$ Raman beams. Therefore, we can design a differential measurement which measures the interferometry phase ϕ_{+1} for $m_F = 1$ states and the interferometry phase ϕ_{-1} for $m_F = -1$ states respectively. The magnetic-field-induced phase is then obtained by the phase difference of the two measurements as $\phi_B = (\phi_{+1} - \phi_{-1})/2$; thus the spatial difference of magnetic field can be measured by this method as

$$\Delta B = (\phi_{+1} - \phi_{-1})/(4\beta T). \quad (2)$$

Furthermore, the differential measurements can reject some systematic errors such as the ac Stark phase shift.

Our atom-interferometry magnetometer is based on an atomic fountain. We use a standard magneto-optical trap (MOT) [23,24] shown in Fig. 2(b) to trap and launch atoms. The vacuum pressure of our aluminum MOT chamber is about 10^{-9} Torr. The top and bottom windows are prepared for the Raman beams to pass through. The ^{87}Rb atoms are released from a rubidium dispenser. The six trapping beams are provided by the laser system (Toptica TA100), which is locked to the ^{87}Rb's crossover peak of $|5S_{1/2},F = 2\rangle \rightarrow |5P_{3/2},F = 2\rangle$ and $|5S_{1/2},F = 2\rangle \rightarrow |5P_{3/2},F = 3\rangle$ by the saturation absorption method. The frequency shift of the trapping beam is controlled by the acoustic optical modulators (AOMs) for loading, launching, and moving molasses. After 1 s of loading time, about 10^8 atoms are trapped and then cooled down in the moving molasses stage to a temperature of 9(1) μK measured with the time-of-flight method. The velocity of atoms after launch is 3.7 m/s, and the maximum height of the atom fountain is 0.7 m. Atoms will enter the interferometry chamber after 230 ms of flying time.

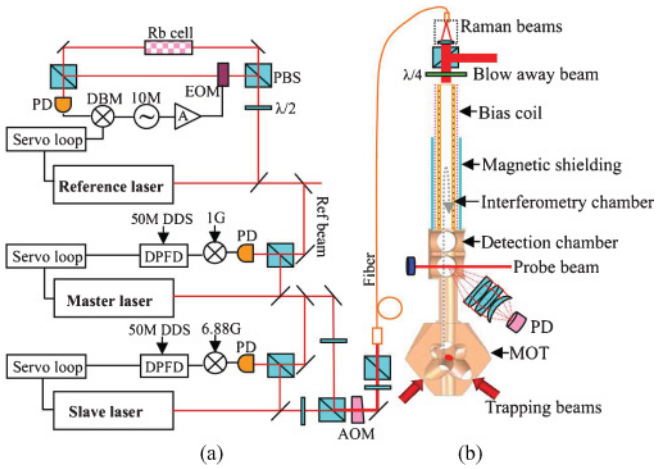

FIG. 2. (Color online) Schematic diagram of the experimental facility. (a) Optics for an OPLL. PD, photo diode; PBS, polarization beam splitter; DBM, double balance mixer; EOM, electric optical modulator; and DDS, direct digital synthesizer. (b) Atom interferometer and the vacuum system.

As shown in Fig. 2(a), the setup of Raman lasers consists of three external-cavity diode lasers (Toptica DL100) operating at around 780 nm. The reference laser (RL) is locked on a ^{87}Rb atomic transition of $|5S_{1/2},F = 1\rangle \rightarrow |5P_{3/2},F = 0\rangle$ using the modulation-transfer (MT) method [25]. This laser constitutes an optical frequency standard and is also used as a repumping laser for MOT. The master laser (ML) is directly frequency locked to the RL with a frequency offset of 1 GHz by an optical phase-locked loop (OPLL) [26]. The slave laser (SL) is phase locked to the ML by another OPLL with a frequency offset of 6.83 GHz, which is the frequency difference between the ^{87}Rb ground-state hyperfine energy levels. Both ML and SL serve as the Raman lasers in the atom-interferometry experiment. In the closed-loop case, the phase noise of the 6.8-GHz beat note within 30–300 kHz measured by a spectrum analyzer is less than −90 dBc/Hz. The main beams of the ML and the SL are overlapped and diffracted by an 80-MHz AOM switch, which is used to control the pulse length. A polarization-maintaining single-mode fiber spatially filters the Raman beams before they are collimated to an e^{-2} diameter of 18.5(1) mm. The Raman beams' output power is 30.0(1) mW, measured at the end of the fiber.

The copropagating $\sigma^+ - \sigma^+$ Raman beams first are used to search the resonance frequency of the transition between the hyperfine magnetic sublevels. When the launched atoms arrive at the interferometry chamber, the resonance frequency is measured by adding a π pulse and scanning the Raman lasers' frequency with a direct digital synthesizer (DDS), where the resonant transitions of $|F = 1,m_F = 0\rangle$ to $|F = 2,m_F = 0\rangle$ and $|F = 1,m_F = 1\rangle$ to $|F = 2,m_F = 1\rangle$ occur at the Raman lasers' offset frequency of 50.000 and 50.112 MHz, respectively. The bias field is estimated to be 80.2 mG with this resonance frequency. We start timing the atom interferometer to measure the interferometry chamber's magnetic field gradient as soon as we obtain the resonance frequency of $m_F = +1$ states. Atoms are first pumped to the $|F = 2\rangle$ state by keeping the repumping laser on for 20 ms after moving molasses. At $t = 223$ ms after launch, a 60-μs-long state selection π pulse is applied to the

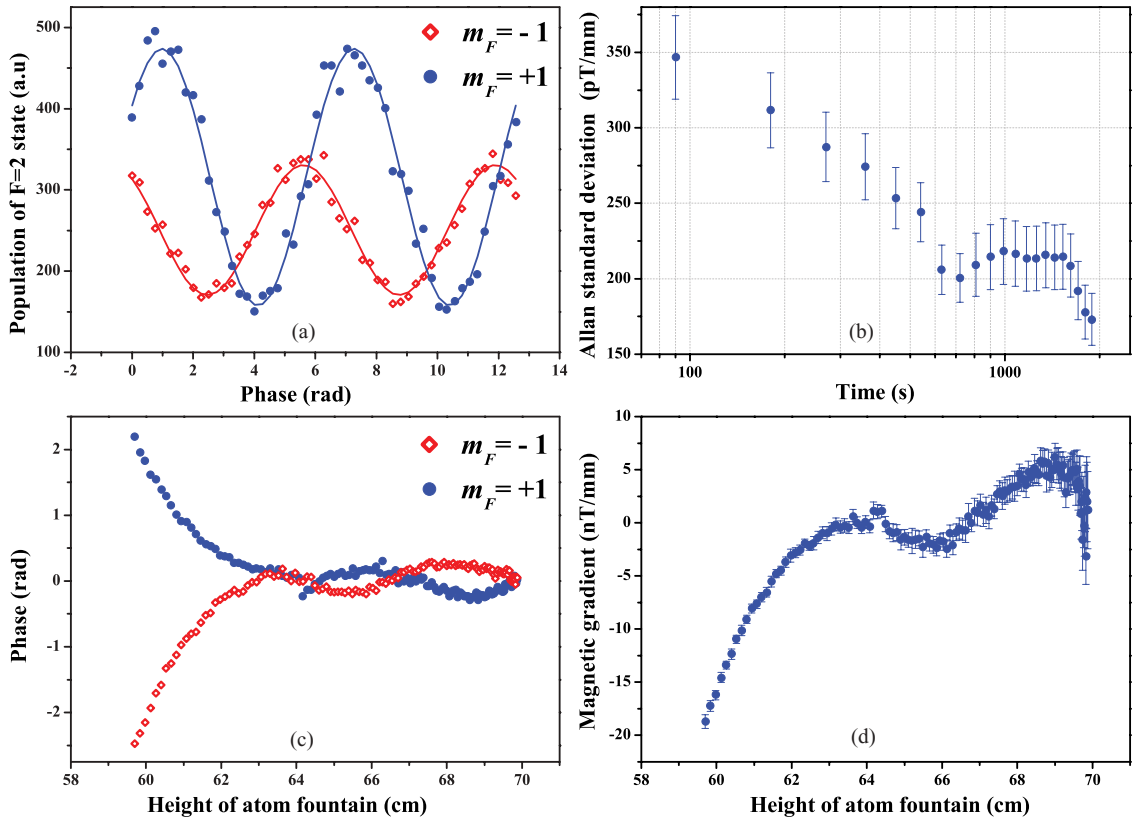

FIG. 3. (Color online) (a) The atom interference fringes for the $m_F = +1$ and $m_F = -1$ states. (b) The Allan standard deviation of magnetic gradient measured by the atom-interferometry magnetogradiometer. (c) The atom interferometer phase for $m_F = +1$ and $m_F = -1$ at different heights of the atomic fountain. (d) The magnetic gradient in the vacuum chamber measured by the atom interferometer.

atoms to transfer the atoms from the $|F = 2, m_F = 1\rangle$ state to the $|F = 1, m_F = 1\rangle$ state. Then 1 ms later, the blow-away beam is turned on for 5 ms to clear the residual atoms in the $|F = 2\rangle$ state. After the state preparation, about 10^6 atoms are prepared in the initial state of $|F = 1, m_F = 1\rangle$ with a purity of more than 90%. At $t = 231$ ms, a $\pi/2$ pulse, following with π and $\pi/2$ pulses with a time interval of $T = 1$ ms, is applied to the atoms. The atom's flying distance between the successive pulses is approximately 1.4 mm. The population of the final state $|F = 2, m_F = 1\rangle$ is recorded by the fluorescence detection system when the atoms fall back to the detection chamber. It takes 1.75 s for a throughout experiment run, including atom loading, state preparation, interferometry process, and detection. The interference fringe is observed via changing the Raman beams' phase of the final $\pi/2$ pulse, and each fringe comprises 51 continuous shots. In order to get a magnetic-induced phase with Eq. (2), the $m_F = -1$ state interference fringe is also observed by manually changing the Raman beams' polarization to $\sigma^- - \sigma^-$ with a quarter-wave plate in about 3 min.

The fringes of $m_F = +1$ and $m_F = -1$ state at $t = 231$ ms are shown in Fig. 3(a). The least-square fitting shows that the phases for $m_F = +1$ and $m_F = -1$ state fringe are $\phi_{+1} = 2.18(4)$ rad and $\phi_{-1} = -2.47(3)$ rad, respectively. This sensitive atom-interferometry magnetic gradiometer was then used to measure the distribution of the magnetic field in the interferometry chamber. We changed the time $t_{\pi/2}$ of the first $\pi/2$ pulse from 231 to 360 ms step by step and finally obtained 130 pairs of interference fringes for both $m_F = +1$ and $m_F = -1$ states at different heights of the atomic fountain. As shown in Fig. 3(c), the blue dots (red diamonds) represent the interference phase for the $m_F = +1$ ($m_F = -1$) state. It can be seen that the phases of the $m_F = +1$ and $m_F = -1$ states are almost inverse. The magnetic gradient $\Delta B_i = (\phi_{-1} - \phi_{+1})/(4\beta T)$ calculated from each pair of fringes is shown in Fig. 3(d). The gradient's error in the top of the fountain is larger than that of the bottom, because the baseline becomes smaller due to the deceleration of the atoms.

The least square fit of $m_F = +1$ state fringe shown in Fig. 3(a) leads to an uncertainty of the interferometer phase $\delta(\phi_{+1})$ of 0.040(6) rad, which gives a resolution of 300(45) pT/mm for the magnetic field gradiometer after 90 s of integration time. The spatial resolution of the gradiometer is about 1.4 mm. The Allan standard deviation of the magnetic gradient is shown in Fig. 3(b). We can see that the resolution could be improved by increasing the integration time. It also tells us that the resolution of the gradiometer at 90 s is 346(35) pT/mm, which is consistent with the result of least squares fit. The current experimental sensitivity of our atom-interferometry magnetic sensor is possibly limited by the magnetic field fluctuation due to the current instability of bias coil.

From the magnetic gradient data, we calculated the magnetic field offset from the first measured point ($t_{\pi/2} = 231$) ms as $B_n = \sum_{i=1}^{n} \Delta B_i$ (black dots in Fig. 4). However, the magnetic field was also obtained by measuring the resonance

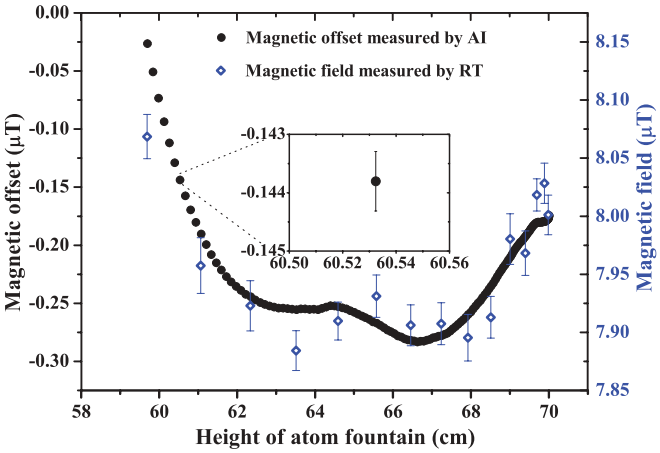

FIG. 4. (Color online) Magnetic distribution in the vacuum chamber measured by atom interferometry (AI) and the magnetic-field-sensitive RT methods.

frequency f_{+1} (f_{-1}) between $|F=1,m_F=+1\rangle$ ($|F=1,m_F=-1\rangle$) and $|F=2,m_F=+1\rangle$ ($|F=2,m_F=-1\rangle$) states with the magnetic-field-sensitive RT method. The value of magnetic field measured by this method is plotted as blue diamonds in Fig. 4 for comparison, and each point of data took about 100 s of measuring time. In this experiment, the resolution of the RT magnetometer is about 20 nT, which corresponds to a resolution of 20 nT/mm for a magnetic gradient measurement at a baseline of 1 mm. We can see that the magnetic field distribution measured with the interferometry method is coincident very well with that obtained with the RT method, while the resolution of the atom-interferometry magnetogradiometer is about 66 times higher than the RT method in mapping the magnetic gradient in this experiment. The resolution of RT magnetometer is limited by determining the resonant frequencies f_{+1} and f_{-1}. Theoretically, the Raman spectroscopy is similar to the spectra of transitions in an atomic clock, which also needs to precisely find the resonant frequency of a two-level atom. The relative uncertainty of the frequency measurements in an atomic clock could be estimated by the Allan standard deviation [27] as $\sigma(t)=1/(QR\sqrt{t})$, where Q is $f/\delta f$, R is the signal-to-noise ratio, and t is the total measurement time. In the case of the RT method, δf is the full width at half maximum of the Raman spectroscopy and is about two times Rabi frequency f_R, and $f=f_{+1}-f_{-1}$. The R due to the atom shot-noise limit for RT method could be written as $\sqrt{N}$, where N is the number of atoms per shot. In our experiment, $f_R\approx 8$ kHz, $f\approx 230$ kHz, and N is about 10^6 per shot, so the potential sensitivity of the RT magnetogradiometer in this experiment is at a level of 1 nT/mm per shot.

The atom shot-noise limit for an atom interferometer's phase resolution is $\sigma\phi=1/\sqrt{N}$ [19], where N is the number of atoms contributing to the interference signal. Given approximately $N=10^6$/shot in our experiment, a phase resolution limited by the shot noise is about 1 mrad. With an atom free evolution time $T=1$ ms, the potential sensitivity of an atom-interferometry magnetic field gradiometer will be at a level of 10 pT/mm per shot.

In conclusion, we have demonstrated an atom-interferometry magnetic gradiometer with a sensitivity of 300 pT/mm after 90 s of integration time. The differential method using $m_F=+1$ and $m_F=-1$ states was used to extract the magnetic field gradient signal, and the common mode rejects some systematic errors. This sensitive and high-spatial-resolution magnetic gradiometer can be used to measure the magnetic field gradient in a vacuum system and correct the systematic error due to magnetic field inhomogeneity in an atom-interferometry gravimeter.

This work is partly supported by the National Basic Research Program of China (Grant No. 2010CB832806) and the National Natural Science Foundation of China (Grant No. 10875045).

[1] A. Sunderland *et al.*, Rev. Sci. Instrum. **80**, 104705 (2009).
[2] T. R. Clem, Naval Engineers J. **110**, 139 (1998).
[3] R. Stolz *et al.*, Leading Edge **25**, 178 (2006).
[4] C. D. Gratta *et al.*, Rep. Prog. Phys. **64**, 1759 (2001).
[5] G. M. Harry *et al.*, Appl. Phys. Lett. **76**, 1446 (2000).
[6] I. K. Kominis *et al.*, Nature (London) **422**, 596 (2003).
[7] P. D. D. Schwindt *et al.*, Appl. Phys. Lett. **85**, 6409 (2004).
[8] S. Xu *et al.*, Rev. Sci. Instrum. **77**, 083106 (2006).
[9] C. Affolderbach *et al.*, Appl. Phys. B **75**, 605 (2002).
[10] A. Peters *et al.*, Nature (London) **400**, 849 (1999).
[11] T. L. Gustavson *et al.*, Phys. Rev. Lett. **78**, 2046 (1997).
[12] J. B. Fixler *et al.*, Science **315**, 74 (2007).
[13] G. Lamporesi *et al.*, Phys. Rev. Lett. **100**, 050801 (2008).
[14] K. Shinohara, T. Aoki, and A. Morinaga, Phys. Rev. A **66**, 042106 (2002).
[15] D. S. Weiss *et al.*, Appl. Phys. B **59**, 217 (1994).
[16] H. Muller *et al.*, Nature (London) **463**, 926 (2010).
[17] J. P. Davis and F. A. Narducci, J. Mod. Opt. **55**, 3173 (2008).
[18] G. R. White *et al.*, J. Mod. Opt. **56**, 2013 (2009).
[19] A. Peters *et al.*, Metrologia **38**, 25 (2001).
[20] K. Moler *et al.*, Phys. Rev. A **45**, 342 (1992).
[21] P. R. Berman ed., *Atom Interferometry* (Academic Press, New York, 1997).
[22] D. A. Steck, Rubidium 87 D Line Data [http://steck.us/alkalidata].
[23] H. J. Metcalf and P. van der Straten, J. Opt. Soc. Am. B **20**, 887 (2003).
[24] M. K. Zhou *et al.*, Front. Phys. China **4**, 170 (2009).
[25] J. L. Hall *et al.*, Appl. Phys. Lett. **39**, 680 (1981).
[26] A. M. Marina and C. R. Stroud, Rev. Sci. Instrum. **79**, 013104 (2008).
[27] A. Bauch and H. R. Telle, Rep. Prog. Phys. **65**, 789 (2002).